Investigation of the APOLLO Fiducial Diffuser

Laura Tom

September 10, 2004

1 Introduction

In order to accomplish the task of measuring the earth-moon distance to millimeter precision, the Apache Point Observatory Lunar Laser-Ranging Operation (APOLLO) must contend with and limit the uncertainties that arise from its complex system. These uncertainties include the retro-reflector array orientation, the laser pulse shape, the detector, and the timing electronics, all of which contribute to an estimated error between 20 and 310 picoseconds (Strasburg 2004). The fiducial photons from the corner cube mounted in the telescope play an important role in each of the components that contribute to the error budget. Besides determining the firing time of the laser, and serving as the basis for a differential measurement for the lunar photons, the fiducial photons also allow for a temporal characterization of the laser pulse shape, the detector, and the timing electronics. Thus, an accurate measurement of the fiducial photons is crucial.

1.1 The Bias Problem

The APOLLO apparatus uses an array of avalanche photodiodes (APDs) to detect the fiducial and lunar photons. A photon's arrival onto the detector would initiate an avalanche of ionizing atoms, and when the current reaches a pre-set level, the accompanying APOLLO electronics produces a digital pulse. A detailed description of APD behavior and electronics can be found in Jana Strasburg's Ph.D dissertion. As part of her thesis research at the University of Washington, Strasburg experimentally characterized the spatial variation of the avalanche photodiode (APD) temporal parameters, including the Gaussian amplitude, A, the Gaussian mean, μ, and the Gaussian spread, σ, for the 20 and 30 micron detectors at wavelengths of 668 and 732 nm. She discovered that APD avalanches that are initiated near the edge of the detector reach the trigger-current more slowly than APD avalanches that are initiated closer to the center of the detector. Thus, a photon hitting the edge of the detector takes longer to trigger than a photon hitting near the center, even if the two photons reached the detector simultaneously. She concluded that the temporal walk of the Gaussian mean created a center-to-edge difference of approximately 250 ps for the 30 micron device, and 120 ps for the 20 micron device.

The center-to-edge difference would not matter if the lunar photons and the fiducial photons both hit the detector in a random spread. Unfortunately, that is not the case for the fiducial photons. Every point on the primary mirror maps onto a certain point on the APD, because the image focused onto the APD is basically a scaled-down image of the primary mirror. Thus, the corner cube's stationary location on the primary mirror dictates

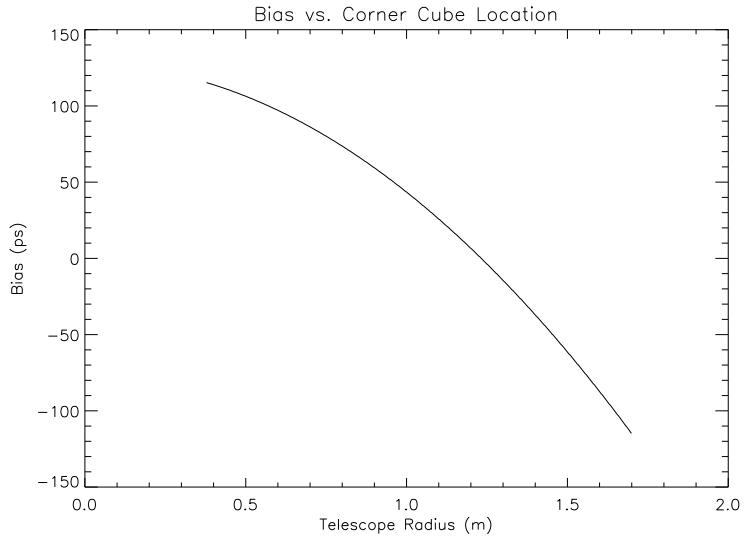

Figure 1: Bias vs. radius

that its return photons map onto a single, small point on the APD, whereas the lunar photons hit the primary mirror in a spread out, random distribution. So if the fiducial photons were to hit the same spot on the detector each time, as was originally planned, a significant bias would be introduced to the time measurements due to the existence of a temporal walk associated with avalanche initiation location. Figure 1 shows the bias as a function of corner cube placement on the primary mirror. If the corner cube were to be placed at the edge of the primary mirror ($\sim$1.70 m) or at the edge of its central obstruction ($\sim$0.38 m) so that our impact to other telescope users is minimal, we get a bias of approximately 115 ps. This resulting bias is a significant setback to APOLLO's efforts to limit the error.

1.2 Solution to the Bias Problem

The proposed solution to the bias caused by the avalanche initiation location is to add a diffuser (such as ground glass) to the optical system. The diffuser would be placed directly behind the pinhole in the receiver's spatial filter and $\sim$150 mm from the collimating lens (fig 2). The ground glass would scatter the fiducial photons, and make them appear to originate from all positions on the telescope's primary mirror—as do the lunar photons—thereby preventing the fiducial photons from hitting the same spot. But to produce the most random photon spread, we would need a diffuser that illuminates the APD as uniformly as possible, and hence, one that produces a large angular spread.

In addition to reducing the temporal bias, the diffuser would also help reduce the strong-signal bias by acting as an additional attenuator in the system. A signal bias naturally occurs since an APD element will only respond to the first photon that reaches it. Hence, in strong signals, we would detect only the photons from the forefront of incoming fiducial returns.

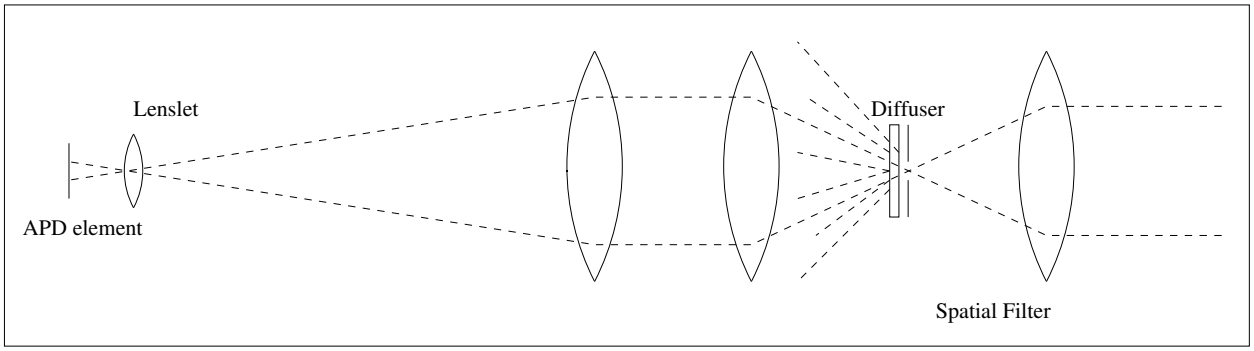

Figure 2: optics

This creates a signal bias from the strong-signal, whereas we want to detect fiducial photons that will reproduce the parent distribution, which happens only with a weaker signal.

Though the ground glass would reduce the bias to acceptable ranges by scattering the photons across the detector, it will adversely affect the jitter because it will introduce a range of avalanche initiation offsets. Now that the fiducial photons can initiate an avalanche in any part of the APD, the laser shape (which can be more easily characterized by fiducial photons when they hit the same spot on the detector) is blurred because of the center-to-edge difference in APD response time. We then come upon the conundrum of correcting for one problem (bias), but contributing to another (jitter). Is it more important to get rid of the bias or keep the jitter low? Fortunately, there is a solution that will enable us to correct the bias and get around the jitter that the diffuser would create. Rather than just having ground glass, one could implement a circular glass piece—a quadrant diffuser that will be operated by a stepper motor synchronized to the laser fire pattern. The glass has four quadrants on its surface: one quadrant is the diffuser; another quadrant is a fixed attenuator with an optical density around 1.0; and two opposite quadrants are clear and thus have no effect on the photons (these two will be used for the lunar photons). Rather than having the fiducial returns go through the ground glass for each laser pulse, they would only go through the ground glass every other pulse. For the remaining fires, the fiducial photons would go through the surface with the fixed optical density so that the fixed attenuator effectively attenuates the same number of photons as the ground glass. Unlike the diffuser, this quadrant would allow the photons to hit a single location on the detector, allowing us to see the laser shape, characterize our system's temporal response, and reduce temporal jitter. Combining the results from the diffuser and the fixed attenuator will allow for the millimeter precision that we seek in an unbiased manner.

The question, then, is how well do these efforts compensate for the temporal walk? Using Jana Strasburg's data, results from experiments done at the UCSD laboratory, and numerical models written with the C programming language, I have attempted to study the diffuser's role in APOLLO. The remainder of this paper will be focused on characterizing the diffuser, and its associated jitter and bias.

2 Characterization of Diffusers

2.1 Experimental Procedure and Results

Four different diffusers have been studied so far: opal glass and 200-grit ground glass from Edmund Industrial Optics, and 25-grit and 50-grit ground glass from the Reynard Corporation. Using a 633 nm helium-neon laser and a Melles Griot calibrated photodiode silicon detector, we measured the flux through each sample of ground glass from an angular position of -45 degrees to 45 degrees. Furthermore, we also measured the flux for the 25-grit and 50-grit ground glass for a laser beam that first goes through a 400 μm pinhole (which simulates the ultimate configuration of the APOLLO receiver), and we tested alternate positions of the ground glass relative to the pinhole. The latter experiment addresses the concern that the diffuser might have irregularities on its surface and cause a splotchy illumination pattern—which presents another source of uncertainty. However, all our trials at various positioning have given us comparable results. The concern of irregularities is also lessened with a look at the ground glass through a microscope, which reveals a rather uniform surface with no apparent irregularities. We also used a green 532 nm laser pointer in one trial, since the laser at Apache Point Observatory has a wavelength of 532 nm. Its results—namely the angular spread—are also comparable to the rest of the data taken with the 633 nm helium-neon laser. We can be assured that the wavelength of the laser beam does not play a significant role in the resulting illumination pattern, and so findings from the experiments done with the helium-neon laser can safely be applied to the APOLLO apparatus.

The flux for each diffuser sample was modeled, revealing that the illumination pattern for each of the ground glass samples (pinhole, non-pinhole, at all illumination positions) had a Gaussian distribution while the opal glass had a Lambertian ($\cos\theta$) distribution. The spread for each sample is shown in Table 1, and a diagram of the Gaussian distribution for one of the frosted ground glass samples is shown in Figure 3. On average, the Edmund 200-grit ground glass has a Gaussian spread, σ, of 7.5°, the 25-grit samples had a σ of 6.0°, and the 50-grit ground glass samples had a σ of about 6.7° . As to which would serve as the best diffuser, we assume that the one with the largest spread would do the best job, since that corresponds to a more uniform illumination pattern that most resembles the random distribution of the lunar photons—and therefore a lower bias. The opal glass, which has the flattest curve at the peak, would work best in this regard. However, fabrication considerations push us to ground glass. We have opted for the 50-grit ground glass, with a Gaussian spread of about 6.5°, which will be the value used throughout the calculations to follow. As will be presented in Section 3, the ground glass works well for our purposes.

2.2 Flux Calculations

The data collected in the diffuser experiments was then used to calculate the forward flux of the system, the intensity of the scattered beam, and the effective optical density of the ground glass within the APOLLO apparatus. The Gaussian intensity at any given angle, θ,

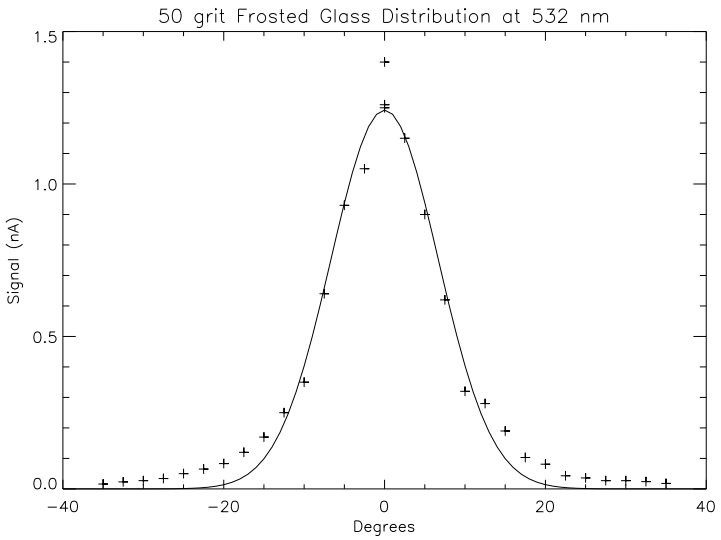

Figure 3: A Gaussian plotted over the illumination pattern of one sample of the 50 grit frosted glass. The flux was measured for every 2.5°.

Description	Sample	Pinhole	Alternate Positioning	σ (degrees)
25-grit	1			5.74
25-grit	2			6.32
25-grit	3			6.22
25-grit	1		X	6.42
50-grit	1			6.83
50-grit	2			6.14
50-grit	3			6.69
50-grit	1		X	6.78
25-grit	1	X		6.35
25-grit	1	X	X	5.26
50-grit	1	X		7.31
50-grit	1	X	X	6.98
50-grit	1	X		6.38
50-grit	1	X	X	6.46
50-grit†	1	X		6.67
200-grit	1			7.48

Table 1: Gaussian spread of sample diffusers. † indicates use of 532 nm laser pointer

Diffuser	I_{input} (mW)	I_{for} (mW)	$I_{\frac{20}{150}}/I_{\text{input}}$	$\log_{10} I_{\frac{20}{150}}/I_{\text{input}}$
200-grit	1.218	0.694	0.071	−1.147
Opal	1.218	0.643	0.002	−2.633
50-grit †	2.763	1.756	0.092	−1.038
50-grit ‡	2.763	1.917	0.104	−0.983

† sample 1 ‡ sample 3

Table 2: Diffuser flux measurements

from the optical axis, is given by,

$$I(\theta) = I_0 e^{-\frac{\theta^2}{2\sigma^2}},$$

where I_0 is the flux at 0° found by

$$I_{\text{meas}}(0^\circ) = \pi I_0 (d^2/4r^2),$$

and r is the distance from the diffuser to the aperture of the photodiode, and d is the diameter of that aperture. Note that d must be much, much smaller than r. In our experiments, the aperture diameter was 3.42 mm for the 200-grit and opal glass, and 2.92 mm for the 50 grit samples. The distance, r, was 125.18 mm for the 200-grit and opal glass, and 110.85 mm for the 50 grit frosted glass samples. The forward flux is consequently the integral of this intensity from 0 to $\frac{\pi}{2}$. This works out analytically to

$$I_{\text{for}} = 2\pi I_0 \sigma^2 (1 - e^{-\frac{\pi^2}{8\sigma^2}}).$$

However, into a larger aperture d (say, the collimating lens), the flux is

$$I_{\text{aper}} = 2\pi I_0 \sigma^2 (1 - \exp(-\frac{\arctan^2(d/2r)}{2\sigma^2}).$$

In the APOLLO optical system, the distance, r, from the diffuser to the collimating lens is 150 mm, with the lens having an aperture, d, of 20 mm. The resulting calculations are shown in Table 2. For the 50-grit ground glass that we plan to use on the quadrant diffuser, the average of the samples have an optical density of approximately 1.01.

However, the calculations above do not take into account any central obscuration, like the obstruction in the center of the 3.5 m telescope. Furthermore, depending on the position of the corner cube in front of the primary mirror, the beam passing through the pinhole of the spatial filter will have an angular offset with respect to the optical axis of up to four degrees. This offsets the center of the Gaussian illumination distribution on the APD. Taking into account a central obstruction, and an angular offset, ψ_0, the intensity at a given angle, ψ, is found by the function

$$I(\psi) = I_0 e^{-\frac{(x-x_0)^2+y^2}{2\sigma^2}},$$

ψ_0	$\frac{I}{I_{\text{input}}}$	$\log_{10}\frac{I}{I_{\text{input}}}$
0.00	0.0902	−1.0446
0.50	0.0900	−1.0458
1.00	0.0893	−1.0493
1.50	0.0881	−1.0552
2.00	0.0864	−1.0634
2.50	0.0843	−1.0740
3.00	0.0819	−1.0869
3.50	0.0790	−1.1022
4.00	0.0759	−1.1198

Table 3: Intensities and optical densities after taking into account an angular offset,ψ_0, and a central obscuration

with $x = \psi\cos\phi$, $\psi^2 = x^2 + y^2$, x_0 identified with ψ_0, and ϕ as an azimuthal angle. The flux is then

$$I_{\text{tot}} = \int_0^{2\pi}\int_{\psi_{\min}}^{\psi_{\max}} I_0 e^{-\frac{\psi^2}{2\sigma^2}} e^{\frac{\psi_0\psi\cos\phi}{\sigma^2}} e^{-\frac{\psi_0^2}{2\sigma^2}}\psi d\psi d\phi,$$

where $\psi_{\min}$ and $\psi_{\max}$ are the inner and outer edges of the illumination pattern on the detector. The integral is not analytic, so a C program was written to numerically integrate this function. The intensities and optical densities calculated from this C program for an illumination pattern with an inner edge at 3.2 μm and an outer edge at 14.4 μm can be found in table 3.

The diffuser and the fixed attenuator must attenuate roughly the same number of photons in order to avoid differing strong-signal biases. Thus, the optical densities that we found will be used to set the value for the fixed attenuator in the quadrant opposite the diffuser. Since the neutral density of the diffuser after taking a central obstruction into account only varies by less than 0.1, we can tolerate angular offset of the Gaussian produced by the ground glass without worrying about a flux mismatch.

3 Calculation of Time Bias and Jitter

From Jana Strasburg's parabolic fits of the spatial dependence of the Gaussian mean, we see that the radial distribution of avalanche delay can be characterized as

$$\tau(r) = Ar^2.$$

The general form of this fit function will be motivated in Section 4 describing a model for the temporal evolution of the avalanche process. Before the calculations for the average delay, bias, and jitter can be done, we needed to find the value of the coefficient, A. We found that A equals 1.17 ps μm^{-2} after plotting the raw data from Jana Strasburg's experiments

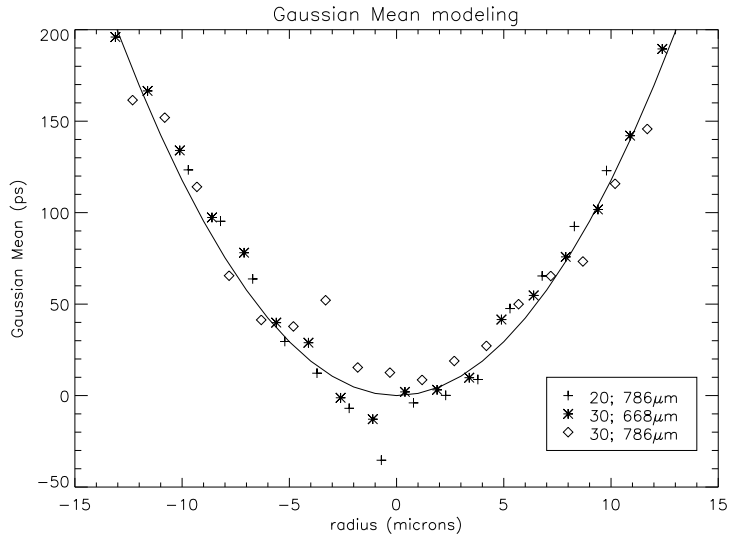

Figure 4: experimental data and the parabolic fit $\tau(r) = 1.17r^2$.

with the 20 micron detector at 786 nm, and the 30 micron device at both 668 nm and 786 nm together, and performing a least squares analysis. Figure 4 shows the raw data and the parabolic fit, $\tau(r) = 1.17r^2$. The mean offset is 1.72 ps. The data from the 20 micron detector at 668 nm was left out from the least squares analysis because it did not appear to be consistent with the others for unknown reasons. However, since we are still representing both wavelengths and both the 20 and 30 micron detectors, the fit is representative of the general case.

The average avalanche delay, $\langle\tau\rangle$, under a non-uniform illumination scheme, $I(r)$, then, is the average of the temporal delay weighted by area:

$$\langle\tau\rangle = \frac{\int_{R_1}^{R_2} \tau(r)I(r)rdr}{\int_{R_1}^{R_2} I(r)rdr},$$

where R_1 and R_2 are the inner and outer edges of the illumination pattern on the detector, and $\tau(r)$ is the delay at a radius r of an avalanche, as discussed above.

Since we have characterized the illumination pattern, the radial distribution of avalanche delay, and the average delay, we can now piece together all the components and finally calculate the bias and the jitter. We define the jitter, σ_τ, or the uncertainty in the avalanche report of a single event, as

$$\sigma_\tau = \sqrt{\langle\tau^2\rangle - \langle\tau\rangle^2}.$$

We have defined the bias as the difference between the average delay for a uniform illumination scheme and the average delay for a non-uniform illumination scheme (in this case, the diffuser has a Gaussian distribution)

$$\text{bias} = \langle\tau\rangle_{\text{uniform}} - \langle\tau\rangle_{\text{Gaussian}}.$$

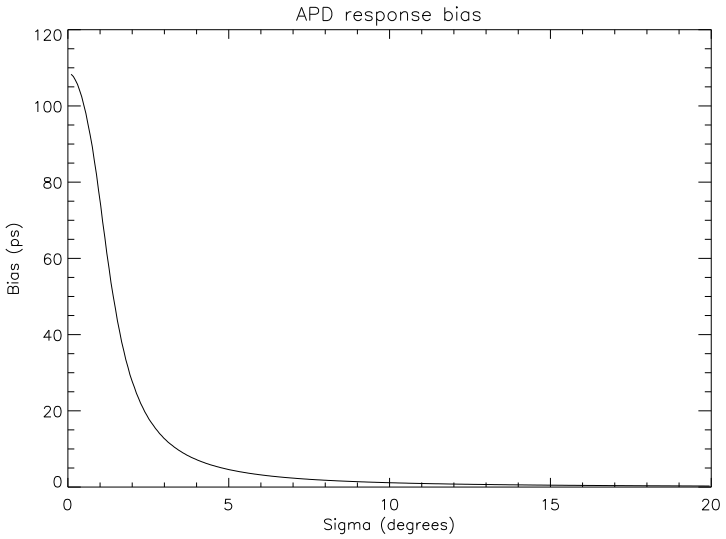

Figure 5: Bias as a function of Gaussian spread, σ.

Figure 5 shows the bias with increasing Gaussian spread, σ. The bias decreases as the Gaussian spread increases, which is expected, because a more uniform illumination pattern would better resemble the lunar photons in regards to the random nature of where they hit the APD. The bias drops significantly between 0° to 2° and then drops under our target bias of 10 ps at a σ of approximately 3.5°. For our ground glass with a σ of 6.5°, the bias is roughly 3 picoseconds, so the temporal walk of the detector is really no longer much of a concern if we decide to use this diffuser. Figure 6 shows the jitter with increasing σ. The jitter levels off at roughly 67 picoseconds, at a σ of roughly 3.0°, so we can conclude that choosing a diffuser with a larger Gaussian spread will not affect the jitter beyond a certain point.

However, the bias and jitter calculations above were done with an ideal situation in mind. In reality, the Gaussian illumination pattern is not centered with respect to the lunar pattern. Taking these offsets into account, the diffuser's Gaussian illumination integral is now

$$I = \int_0^{2\pi} \int_{R_1}^{R_2} e^{-\frac{r^2}{2\sigma^2}} e^{\frac{r\psi_0 \cos\phi}{\sigma^2}} r dr d\phi.$$

Furthermore, imperfect alignment of the lenslet and/or APD would result in an illumination pattern that is shifted off-center with respect to the APD (see fig. 7. The delay associated with an event at a radius, r, at an angle, ϕ, under the conditions of a 2-D displacement centered at (δ_x, δ_y), is given by

$$\tau(r, \phi) = A(r^2 + 2r\delta_x \cos\phi + 2r\delta_y \sin\phi + \delta_x^2 + \delta_y^2),$$

where $A = 1.17$ ps μm^{-2} as mentioned earlier. With these offsets, another C program was written to recalculate the bias and jitter. Table 4 lists the bias for each Gaussian and APD

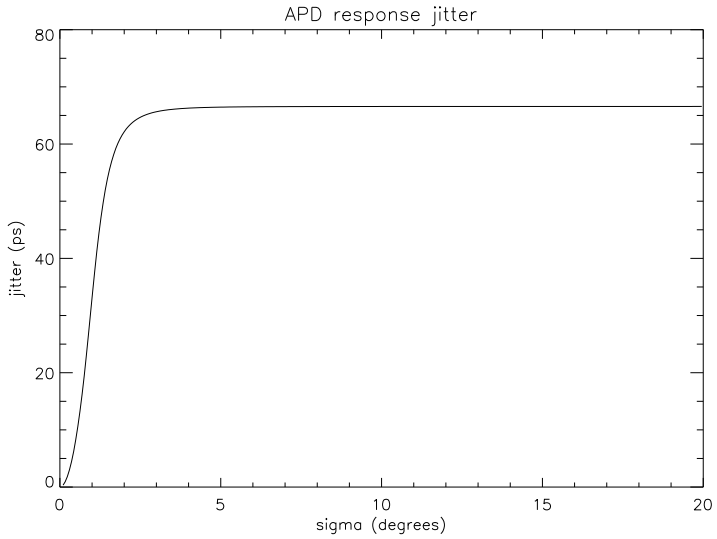

Figure 6: Jitter as a function of Gaussian spread, σ.

offset, and Table 5 lists the jitter for each Gaussian and APD offset. Figure 8 is a diagram of the bias as a function of these offsets. The behavior of the bias does not show much variation. At the largest offset case at 4° with an avalanche centered at (−4,0) microns, the bias is only 7.5 picoseconds, still well under the target of 10 picoseconds. The jitter also does not show much variation, and remains relatively steady, not going above 73 picoseconds.

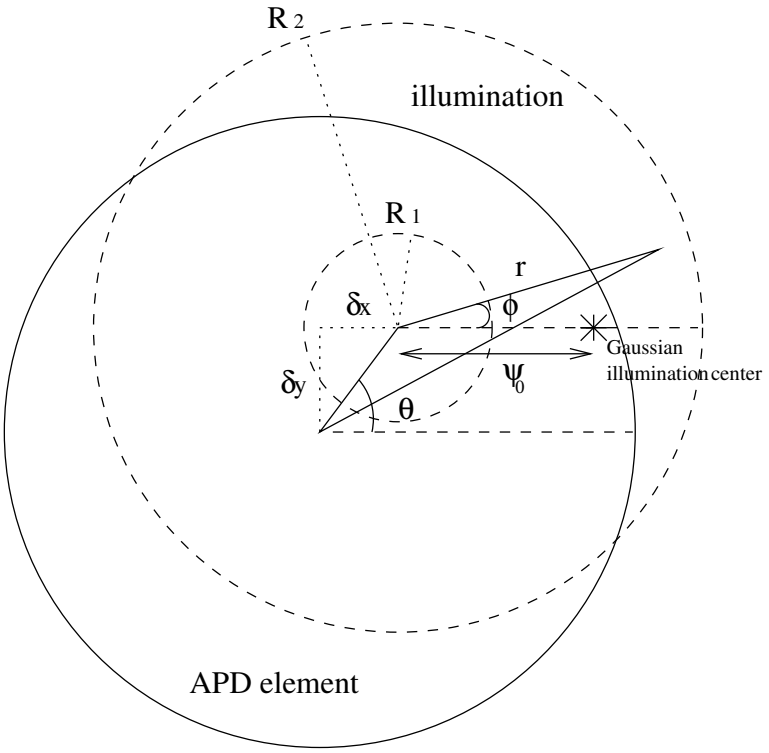

Figure 7: Geometry of an off-center illumination pattern on the APD

ψ_0	$(-4,0)$	$(-4,2)$	$(-4,4)$	$(-2,0)$	$(-2,-2)$	$(-2,4)$	$(0,0)$	$(0,2)$	$(0,4)$	$(2,0)$	$(2,2)$	$(2,4)$	$(4,0)$	$(4,2)$	$(4,4)$
0.00	1.766	1.558	1.039	2.613	2.274	1.558	3.058	2.613	1.766	2.613	2.274	1.558	1.766	1.558	1.039
0.25	2.137	1.913	1.355	2.858	2.492	1.739	3.056	2.616	1.771	2.364	2.061	1.386	1.392	1.207	0.733
0.50	2.506	2.266	1.668	3.099	2.707	1.917	3.049	2.614	1.772	2.112	1.844	1.211	1.017	0.854	0.424
0.75	2.872	2.616	1.977	3.337	2.917	2.090	3.038	2.607	1.767	1.857	1.623	1.031	0.639	0.498	0.111
1.00	3.237	2.964	2.283	3.572	3.124	2.259	3.022	2.595	1.758	1.598	1.398	0.846	0.259	0.139	-0.203
1.25	3.598	3.309	2.585	3.803	3.327	2.424	3.001	2.579	1.744	1.337	1.170	0.658	-0.123	-0.221	-0.522
1.50	3.957	3.650	2.885	4.030	3.525	2.584	2.976	2.557	1.725	1.072	0.937	0.465	-0.507	-0.585	-0.845
1.75	4.314	3.990	3.181	4.254	3.720	2.740	2.947	2.531	1.701	0.803	0.701	0.268	-0.893	-0.951	-1.170
2.00	4.668	4.326	3.473	4.474	3.911	2.891	2.913	2.500	1.673	0.532	0.461	0.067	-1.282	-1.319	-1.498
2.25	5.019	4.659	3.762	4.691	4.098	3.038	2.874	2.464	1.639	0.257	0.218	-0.138	-1.672	-1.690	-1.829
2.50	5.368	4.989	4.048	4.903	4.280	3.181	2.831	2.424	1.601	-0.019	-0.028	-0.347	-2.064	-2.063	-2.164
2.75	5.714	5.317	4.330	5.112	4.459	3.319	2.784	2.379	1.558	-0.300	-0.279	-0.560	-2.458	-2.438	-2.501
3.00	6.057	5.641	4.608	5.318	4.634	3.453	2.732	2.329	1.510	-0.584	-0.533	-0.778	-2.854	-2.816	-2.841
3.25	6.398	5.963	4.883	5.519	4.804	3.582	2.676	2.274	1.458	-0.870	-0.791	-0.999	-3.251	-3.196	-3.184
3.50	6.736	6.281	5.154	5.717	4.970	3.707	2.615	2.215	1.400	-1.160	-1.052	-1.225	-3.650	-3.577	-3.529
3.75	7.071	6.596	5.422	5.911	5.133	3.828	2.550	2.151	1.338	-1.452	-1.316	-1.454	-4.051	-3.961	-3.878
4.00	7.403	6.908	5.686	6.102	5.291	3.944	2.480	2.082	1.272	-1.748	-1.584	-1.687	-4.453	-4.347	-4.229

Table 4: Bias in picoseconds with off-center Gaussian illumination patterns (ψ_0), in degrees, combined with offset APD/lenslet (δ_x, δ_y), in μm.

ψ_0	$(-4,0)$	$(-4,2)$	$(-4,4)$	$(-2,0)$	$(-2,-2)$	$(-2,4)$	$(0,0)$	$(0,2)$	$(0,4)$	$(2,0)$	$(2,2)$	$(2,4)$	$(4,0)$	$(4,2)$	$(4,4)$
0.00	69.486	70.334	72.749	67.365	67.897	70.333	66.563	67.373	69.484	67.365	67.898	70.333	69.486	70.334	72.749
0.25	69.373	70.239	72.684	67.260	67.821	70.290	66.563	67.375	69.491	67.468	67.979	70.389	69.597	70.435	72.827
0.50	69.259	70.142	72.618	67.155	67.744	70.248	66.563	67.378	69.498	67.570	68.061	70.444	69.706	70.534	72.904
0.75	69.142	70.043	72.550	67.049	67.667	70.205	66.563	67.382	69.506	67.671	68.141	70.500	69.813	70.631	72.980
1.25	68.903	69.841	72.413	66.834	67.511	70.120	66.564	67.389	69.522	67.870	68.300	70.610	70.021	70.821	73.128
1.50	68.780	69.738	72.343	66.728	67.432	70.078	66.565	67.394	69.531	67.968	68.379	70.665	70.122	70.913	73.200
1.75	68.656	69.634	72.273	66.612	67.353	70.035	66.566	67.399	69.540	68.064	68.457	70.719	70.220	71.003	73.271
2.00	68.531	69.528	72.201	66.505	67.274	69.992	66.566	67.404	69.550	68.160	68.535	70.773	70.317	71.092	73.341
2.25	68.403	69.420	72.129	66.394	67.194	69.950	66.567	67.409	69.559	68.254	68.611	70.827	70.411	71.179	73.409
2.50	68.274	69.312	72.056	66.283	67.114	69.907	66.568	67.415	69.570	68.347	68.687	70.880	70.504	71.264	73.477
2.75	68.143	69.202	71.982	66.170	67.034	69.865	66.570	67.421	69.580	68.438	68.762	70.933	70.594	71.347	73.542
3.00	68.010	69.090	71.908	66.057	66.954	69.823	66.571	67.428	69.591	68.528	68.836	70.986	70.682	71.428	73.607
3.25	67.876	68.978	71.833	65.943	66.874	69.781	66.572	67.435	69.603	68.617	68.909	71.038	70.767	71.507	73.670
3.50	67.740	68.864	71.757	65.829	66.793	69.739	66.574	67.442	69.614	68.704	68.982	71.090	70.851	71.584	73.731
3.75	67.603	68.749	71.681	65.714	66.712	69.697	66.575	67.449	69.626	68.790	69.053	71.141	70.932	71.660	73.791
4.00	67.464	68.633	71.604	65.599	66.631	69.655	66.576	67.457	69.638	68.875	69.123	71.191	71.011	71.733	73.850

Table 5: Jitter in picoseconds with off-center Gaussian illumination patterns (ψ_0), in degrees, combined with offset APD/lenslet (δ_x, δ_y), in μm.

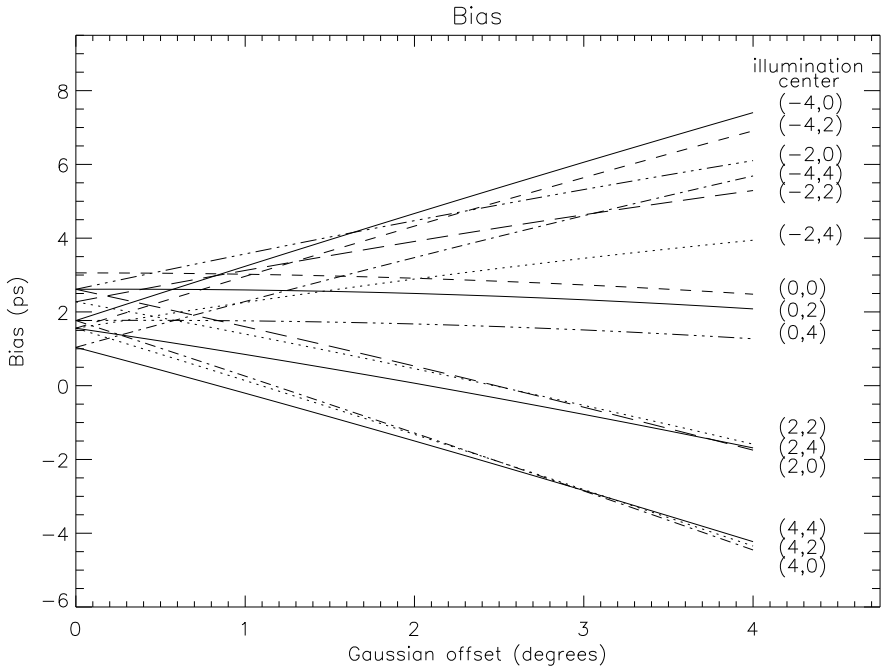

Figure 8: Bias for Gaussian and APD offsets

4 Modeling the Avalanche Initiation Bias

The cause of these concerns over the bias—the temporal delay itself, can be modeled so we can better understand the avalanche process. Though the avalanche delay is characterized as $\tau(r) = Ar^2$ after fitting Jana Strasburg's data, the general form of this fit function is a bit more complicated. The current in an APD avalanche is proportional to the area of the APD avalanche region, so we can model the temporal evolution of the avalanche process by modeling the avalanche area as it grows with time. At a given avalanche radius, ρ, and a given the distance from the APD center to the avalanche center (the initiation location), r, for an APD of radius R (see Figure 11), we have

$$\cos\theta = \frac{R^2 - r^2 - \rho^2}{2r\rho}$$

$$\cos\psi = \frac{R^2 + r^2 - \rho^2}{2rR}.$$

The area of the APD avalanche is then

$$A = \begin{cases} \pi\rho^2 & \rho < R - r \\ \frac{1}{2}(2\pi - 2\theta)^2\rho + \rho^2 \sin\theta\cos\theta + R^2\psi - R^2\sin\psi\cos\psi & R - r < \rho < r + R \\ \pi R^2 & \rho > r + R \end{cases}$$

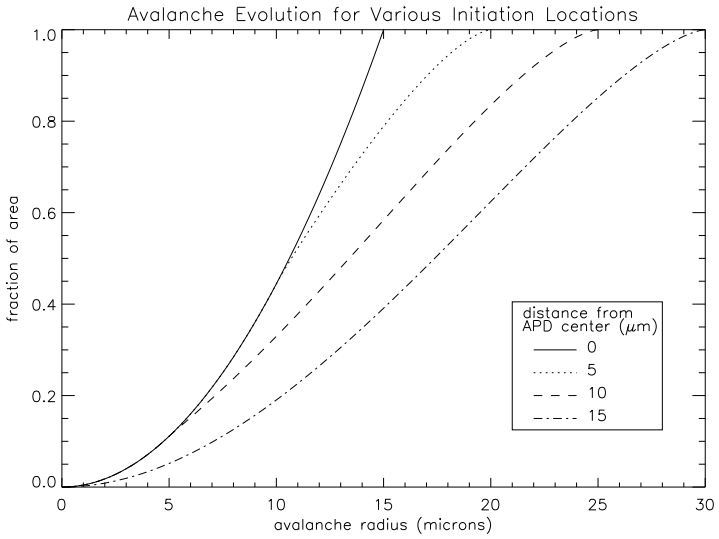

Figure 9: The fractional area of an APD avalanche with respect to the full area of the APD as a function of avalanche initiation location

A C program was written to calculate the fractional area of an APD avalanche with respect to the full area of the APD as a function of the avalanche initiation location. Figure 9 displays the results of this program. The temporal differences for the different initiation locations in achieving a certain fractional area (which corresponds to a threshold trigger-current) are apparent. Furthermore, we can find the speed of growth with the relation,

$$\rho(t) = \alpha t.$$

where ρ is the radius of the avalanche at time t. For an APD with a radius of 15μm, the temporal delay, $\tau(15\mu\text{m})$ is 263 ps. Consequently, our best model would have a temporal walk of 263 ps. we get a temporal walk of 259 ps at a trigger-area-fraction of 0.7 when α is 0.035. Thus, the speed of growth is 0.035 μm ps^{-1}, which is approximately 3.5 times slower than the room temperature thermal velocity of an electron in silicon (0.12 μmps^{-1}). Another C program was written to model the temporal delay by specifically simulating the conditions in Jana Strasburg's experiments. Figure 10 displays the results of this program for a trigger fractional area of 0.7, convolved with a Gaussian with spread of 2.29 microns (this σ is based on the laser RMS reported by Jana Strasburg in her thesis), plotted over the experimental data. The mean offset is 1.96 ps. This model produces a sharp cutoff near the bottom of the parabola that is related to the radius of the avalanche when it reaches the trigger-current.

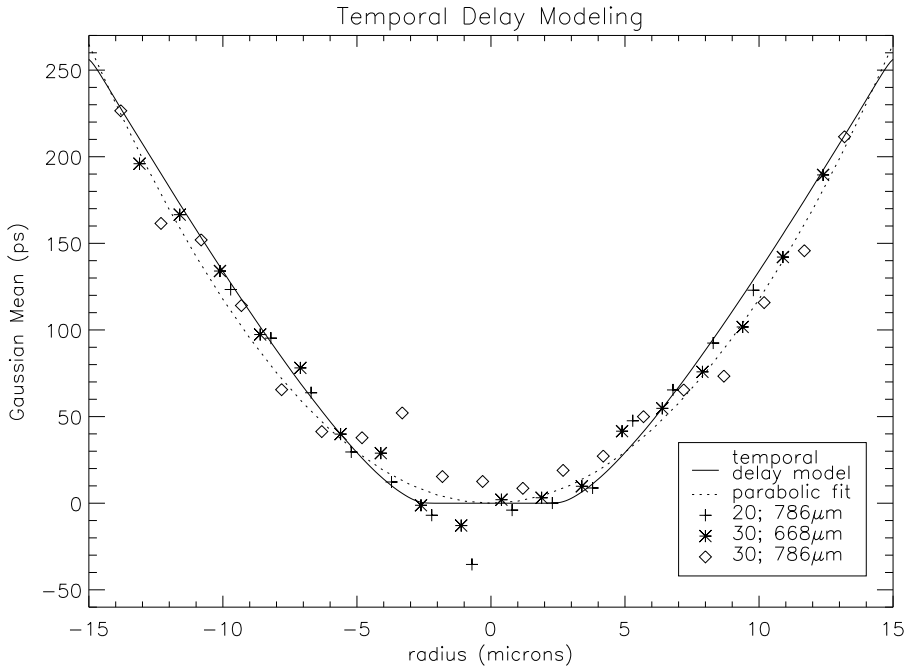

Figure 10: A model of the temporal delay for a trigger fractional area of 0.7, convolved with a Gaussian ($\sigma = 2.29$ microns) with the laser RMS

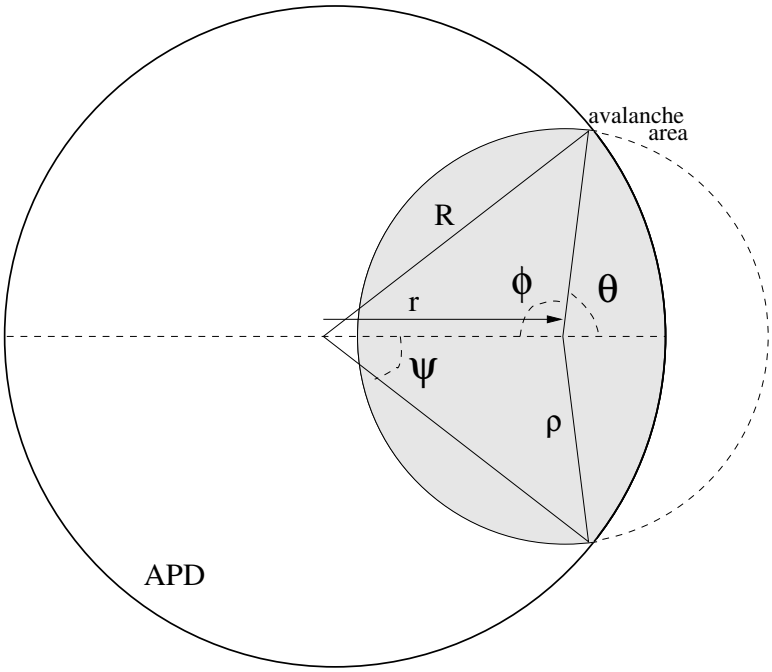

Figure 11: Geometry used to calculate area of APD avalanche (shaded) as a function of ρ

5 Conclusions

The APOLLO fiducial diffuser effectively removes the worries of a timing bias caused by the temporal walk associated with avalanche initiation location within the APD element. We try to make the fiducial photons appear to originate from all positions on the telescope's primary mirror so they would have the same distribution on the detector as the lunar photons. By including a ground glass diffuser with a Gaussian spread of 6.5° into the APOLLO apparatus as proposed, we can cut the bias from 115 ps to just 3 ps—far below the target bias of 10 ps. Additionally, the C program calculations show that even off-centered illumination patterns of up to 4 degrees together with a two-dimensional misalignment of the lenslet with respect to the APD of up to 4 microns in the X and the Y directions yield a bias of under 10 ps. largely insensitive to offset. We can further conclude that the Reynard Corporation 50-grit ground glass having a Gaussian spread of 6.5° works well enough so that further fabrication of other ground glass samples is not necessary. For that matter, we have characterized the Gaussian spread of three different grits of ground glass, to see that the spread does not vary by much from one grit to another. Thus, any additional concern over the fabrication process of the ground glass is also unwarranted.

For us to get rid of the bias without increased jitter, we have combined with the diffuser a fixed attenuator that would allow us maximum performance in our ability to characterize the laser pulse shape and our system's temporal response. In the investigation and characterization of the diffuser, we have found that the value of the optical density for the fixed attenuator should be around 1.0. That way, both the diffuser and the fixed attenuator can attenuate approximately the same number of photons and prevent a strong-signal bias.

Furthermore, we can claim to have a better understanding of the temporal walk with our model of the APD avalanche evolution process. The good fit, indicated by chi-square tests of our model, confirm that our understanding and theory on the temporal walk agree with the experimental findings.

With the solution of a four quadrant disk that diffuses, attenuates, and lets lunar photons pass through unchanged, the discovery of the temporal walk is no longer a cause for concern, and the task of measuring the earth-moon distance to millimeter precision is one step closer to reality.